A host AAA-ATPase exhibits bacteriolytic activity for clearance of microbial infection

Sourav Ghosh[1], Suvapriya Roy[1], Navin Baid[1], Udit Kumar Das[1], Dipasree Hajra[2], Sneha Menon[3], Mohammad Sahil[3], Sudipti Shaw[1], Sumit Rakshit[1], Raju S Rajmani[2], Harikrishna Adicherla[4], Jagannath Mondal[3], Dipshikha Chakravortty[2], Anirban Banerjee[1*]

[1]Department of Biosciences and Bioengineering, Indian Institute of Technology Bombay, Mumbai 400076, Maharashtra, India.

[2]Department of Microbiology and Cell Biology, Indian Institute of Science, Bengaluru 560012, Karnataka, India.

[3]Tata Institute of Fundamental Research, 36/P Gopanapalli Village, Hyderabad 500046, Telangana, India.

[4]CSIR-Centre for Cellular and Molecular Biology, Uppal Road, Habsiguda, Hyderabad 500007, Telangana, India.

*Corresponding author; E-mail: abanerjee@iitb.ac.in; Phone: +(91)-22-25767794. Fax: +(91)-22-25723480.

Summary

An array of cytosol guarding factors impede bacterial invasion and preserve cellular sterility. Amongst them, proteasomal degradation of ubiquitinated pathogens has emerged as a critical mechanism ensuring cytosolic sanctity. But smaller size of the proteasomal barrel and its inability to extract membrane-bound proteins, questions this paradigm. Our study unveiled a unique mechanical force-based strategy, employed by VCP/p97, an AAA-ATPase, which by extracting ubiquitinated bacterial surface proteins, eliminates pathogens. Using molecular dynamic simulation along with *in-vitro* and *ex-vivo* experiments, we demonstrated that p97's segregase activity is central to its bactericidal effect. Assisted by cofactors NPLOC4 and UFD1, p97 causes extensive lysis of phylogenetically diverse microbes and triggers leaching of bacterial cytosolic contents. *In-vivo*, p97 abrogated bacterial proliferation in host tissues and protected animals from lethal infections. Overall, we unravelled a distinct innate immune function of p97, which is critical for host protection against bacterial infections.

Keywords

VCP/p97, AAA-ATPase, Bacterial pathogens, Ubiquitination, Cell autonomous immunity, Proteasome

Introduction

Cell-autonomous immunity consists of a set of evolutionarily conserved, robust self-defense strategies that metazoans employ to guard its cytosol from bacterial invasion. Host cytosol, rich in nutrients, acts as a conduit for sustenance of microbial life. To counteract such fatality, the inheritance of various guarding factors is necessary in both immune and non-immune cells. Eukaryotic host has evolved intricate layers of cytosolic pathogen sensing strategies encompassing various Pattern Recognition Receptors (PRRs) and Damage Associated Molecular Patterns (DAMPs). PRRs recognize diverse Pathogen-associated molecular patterns (PAMPs) that are conserved signatures of the pathogens, such as nucleic acid, lipids, carbohydrates, and peptides[1]. DAMPs on the other hand resemble nonspecific host insults inflicted by pathogens or other sterile damages[2]. Collectively, their sensing triggers effector molecules that participate in pathogen clearance[3]. For example, a major proportion of the invading microbes are subjected to clearance via selective autophagy (Xenophagy) mediated by sensing of galectins which act as an 'eat me signal'[4]. On the other hand, interferon-inducible gene families such as IRG (Immunity-related guanosine triphosphatase) target vacuolar pathogens. IRGM1 binds to phosphoinositol 3,4,5 triphosphate and assists in assembling the 'GKS' effectors onto the pathogenic phagosomes, promoting lysosomal fusion[5, 6]. Similarly, antimicrobial peptides such as the GBP family (Guanylate binding proteins) target the lipopolysaccharides on the Gram-negative bacterial surface[4]. GBPs act as versatile enforcers by rupturing the pathogen as well as forming a signaling platform for the initiation of caspase-4-dependent pyroptosis[7, 8]. Additionally, with the assistance of GBPs, which permeabilizes the pathogen's outer membrane, APOL3 (Apolipoprotein L3), with its detergent-like activity, causes lysis of the bacterial inner membrane, thus rendering them inactive[9]. Moreover, nutrient deprivation by indoleamine 2,3 dioxygenase (IDO) that degrades L-tryptophan restricts microbial growth by limiting critical amino acids[10]. This fine synchronization between a plethora of sensors and executioners forms the decisive fail-safe barrier against a variety of cytosol-invading pathogens.

Pathogenic access to cytosol acts as the spark for initiation of host surveillance mechanisms. Bacteria with an active intracellular life, such as *Salmonella* Typhimurium (STm), or transient intracellular life, such as *Streptococcus pneumoniae* (SPN) and *Streptococcus pyogenes* (GAS), with the help of type III secretion system or pore-forming toxins (pneumolysin, Ply for SPN and streptolysin O, SLO for GAS), causes catastrophic damage to the endosomal membrane and invade the cytosol to flourish[11, 12]. Once in the cytosol, apart from other mechanisms, a large subset of microbes gets ubiquitinated for subsequent elimination. Ubiquitination, a cellular homeostatic process, also acts as a significant innate immune barrier in preserving cytosolic sterility. The ubiquitin machinery, which consisted of E1-, E2-, and E3-

enzymes, synthesize polyubiquitin chains of different topologies on either conventional proteinaceous substrates or non-conventional lipids and carbohydrates present on microbial surface[13, 14, 15]. E3 ligases such as PARKIN, TRIM16, and Nedd4 conjugate K63-Ub linkages on pathogen-containing vacuoles (PCVs) that drive them toward autophagy, whereas LUBAC adds M1 linear ubiquitin chain that activates the NF-κβ pathway[16, 17, 18, 19]. On the contrary, our previous findings suggest that surface proteins of pathogens consist of PAMPs in the form of degron sequences. These degrons are recognized by specific E3 ligases such as SCF^{FBXW7}, which adds K48-polyUb chains to drive their degradation[20]. The existing dogma suggests that such K48 poly-ubiquitinated pathogens are cleared via proteasomal degradation, similar to the K48-ubiquitinated host proteins. Generally, substrates processed by the proteasome are needed to be forced down its barrel, where it is first dismantled and subsequently degraded. However, devouring of an entire bacterium into the proteasome is ambiguous due to the significant difference in size (proteasomal entry portal diameter ~ 10-20 nm[21]; bacterial size ~ 1.5-2 μm). Moreover, bacterial surface proteins that are ubiquitinated, are either cell wall or membrane-bound, posing a challenge for the proteasome to extract it for proteolysis. We therefore speculate that auxiliary host extractors are involved in easing this conundrum.

AAA-ATPase family proteins are known to be notable segregators in all life forms. They are involved in diverse cellular activities, ranging from cellular homeostasis to organellar biogenesis[22]. Remarkably, even though their sequence similarity is low, their structure and the tendency to oligomerize remains highly conserved[23, 24]. Importantly, the walker A motif in the AAA-ATPase normally binds to ATP and walker B motif coordinates with Mg^{2+} to feature its activity[25]. The chemical energy generated by ATP hydrolysis is converted into mechanical force that aids in commencement of its functions. Across the various clade of AAA-ATPase family, most of them lack proteolytic activity and a major subset of them direct unfolded substrates towards the proteasomal machinery for degradation[26].

In this study, we screened various AAA-ATPases based on their cytosolic availability and observed strong association of VCP/p97 (Valosin containing protein), a type II AAA-ATPase with cytosol dwelling microbes. Surprisingly, we found that p97 is a bacteriolytic agent which, while extracting ubiquitinated proteins, forcefully disintegrates membranes of phylogenetically diverse pathogens, triggering release of their internal contents. We also demonstrate that the ATPase activity harnessed by p97 is crucial for such bactericidal activity which by guarding the cytosol hinders bacterial replication and protects the host from severe sepsis.

Results

Discovery of VCP/p97 as an antibacterial AAA-ATPase

Proteasomes have been implicated in maintenance of cytosolic sterility by eliminating ubiquitinated pathogens[27, 28, 29]. However, the apparent size difference between proteasomes and pathogens and the fact that surface bound bacterial proteins need to be extracted before degradation, raises questions about the direct involvement of proteasomes in bacterial clearance. These entail the necessity for an additional aiding factor. AAA-ATPase family proteins are one of the critical extractors with diverse cellular activities. We therefore chose to investigate the role of AAA-ATPase's in extraction of ubiquitinated bacterial surface proteins. Based on the cytosolic availability and involvement in cellular proteastasis, we selected p97, PSMC6 (6th subunit of the 19S ATPase complex), MDN1 (Midasin), VPS4 (Vacuolar protein sorting-associated protein) as potential extractors. We found that in SPN infected host cells, p97 and PSMC6 significantly localized to bacteria (~ 28 and 23%, respectively), while MDN1 (~ 8%) and VPS4 (~ 12%) showed minimal association (Fig.1A, S1A-D). The interaction of these AAA-ATPases with PspA (Pneumococcal surface protein A) which is one of the surface proteins of SPN reported to be ubiquitinated[20], was also assessed by co-immunoprecipitation. Our results suggest that p97 co-precipitated with PspA, whereas other AAA-ATPase displayed little or no interaction (Fig. 1B). Further, decrease in association of p97 (~ 2.3-fold) with SPN mutant lacking ubiquitinable surface proteins (PspA and BgaA) supports our findings (Fig. S2A). This led us to investigate the consequence of p97's targeting to bacterial proteins in real time. Surprisingly, we observed progressive decaying of RFP tagged SPN's fluorescence (~ 50 min) following p97's recruitment onto the bacteria (~ 24 min) (Fig. 1C, D, Movie S1). To verify this unusual role of p97 in bacterial killing, we downregulated its expression using gene specific siRNA (Fig. S3A) and observed ~ 1.8-fold increase in SPN's intracellular persistence (Fig. 1E). We then extrapolated our investigation to figure out whether such defense mechanism is specific for SPN or holds true in case of other pathogens. Indeed, we found that the persistence of two intracellular pathogens, STm and GAS, increased by ~ 2 and 1.5-fold, respectively, after downregulating p97's expression (Fig. 1E). However, lowering expression of PSMC6 did not yield any significant change in bacterial survival (Fig. 1E, S3B). Moreover, inhibition of p97's activity using DBeQ and NMS-873 led to elevated bacterial burden inside host cells (Fig. 1F, S3E-H).

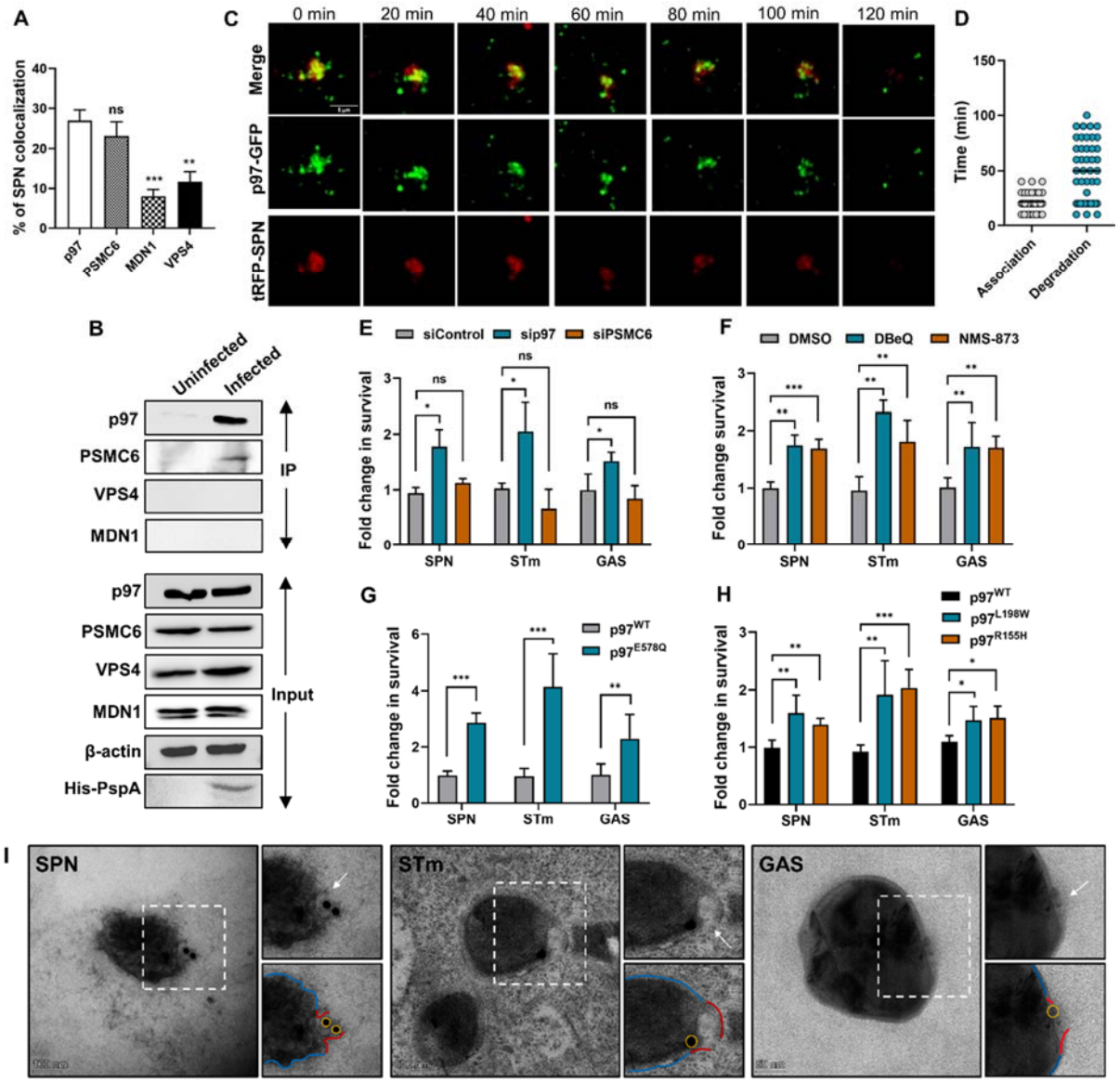

Figure 1. p97 is required to eliminate intracellular pathogens. A. Association of various AAA-ATPases (p97, PSMC6, VPS4, and MDN1) with intracellular SPN. n>100 bacteria/coverslip. **B.** Immunoprecipitation of pneumococcal surface protein PspA following infection of A549s with SPN demonstrates that the bacterial surface component interacts majorly with p97, while PSMC6, VPS4 and MDN1 showed minimal or no interaction. **C.** Time-lapse imaging showcasing the degradation of SPN (red) upon association with p97 (green). **D.** Kinetics of p97 association with SPN and its subsequent degradation after infection of A549 cells. n=35. **E.** Fold change in intracellular survival of SPN, STm, and GAS following transfection of host cells with sip97 and siPSMC6, normalized to scramblase control. **F.** Fold change in survival of intracellular SPN, GAS, and STm after treatment of host cells with p97 inhibitors DBeQ (reversible inhibitor) or NMS-873 (irreversible inhibitor), normalized to DMSO (vehicle). **G-H.** Fold change in survival of intracellular SPN, GAS and STm in host cells expressing $p97^{E578Q}$ (catalytic mutant) **(G)** or $p97^{R155H/R198W}$ (polymorphic mutations

associated with multisystem proteinopathy) **(H)**, normalized to wild type host cells. **I.** Immunogold-transmission electron microscopy demonstrating the localization of p97 specific immunogold particle (25 nm) on ruptured bacterial surface in infected host cells. Scale bar, 100 nm for SPN, 500 nm for STm and 50 nm for GAS.
For all intracellular survival assays, A549s are infected with SPN and GAS for 9 h while HeLa cells were infected with STm for 6 h. Statistical significance was assessed by one-way ANOVA followed by Dunnett's test. Two-tailed unpaired student's t-test (nonparametric) was used for (G). *P < 0.05; **P < 0.01; ***P < 0.005. Data are means ± SD of N = 3 independent biological replicates.

At this stage we hypothesized that though p97 is primarily recruited to the pathogen for extraction of ubiquitinated surface proteins, the pulling force it exerts causes bacterial demise. The relation between force exertion and bacterial killing was demonstrated by using $p97^{E578Q}$, a catalytic mutant of p97 which is unable to generate mechanical force[30]. Cells expressing this mutant form not only had higher K48-Ub substrate accumulation (Fig. S4A) but also failed to clear pathogens, resulting in increased intracellular bacterial burden (~ 2.9, 4 and 2.3-fold in SPN, STm and GAS, respectively) (Fig. 1G). Further, polymorphic mutations in p97 (R155H, L198W), alter its activity, leading to multisystem proteinopathy[31]. We found that cells harbouring these mutant p97 alleles accumulated elevated levels of K48-Ub substrate (Fig. S4B-C) and had diminished ability to clear intracellular pathogens (~ 1.4 to 2-fold) (Fig. 1H). Finally, to evaluate the outcome of p97's extraction ability on bacterial surface, we used immunogold transmission electron microscopy and observed deposition of p97 specific gold particles (25 nm) onto ruptured bacterial surface (Fig.1I). This fuelled our belief that surface protein extraction mediated by p97 may inflict significant damage to the pathogens. Overall, our results hint towards exclusive involvement of p97 in cell autonomous immunity and its unique role in clearance of phylogenetically distinct bacteria by disrupting their membrane.

VCP/p97 targets cytosolic ubiquitinated pathogens

Invasive pathogens by virtue of producing toxins or needle like secretion systems damage the vacuoles encasing them and escape to the cytosol[11, 12]. These cytosolic microbes are sensed by various E3 ligases which decorates pathogen's surface proteins with ubiquitin[14, 18, 20]. Given that p97 is highly abundant in the cytosol and acts on ubiquitin signals, we speculated that it would target the cytosolic bacterial population. Indeed, using structural illumination microscopy we observed that ~ 75%, 66%, and 48% of p97 positive SPN, STm, and GAS, respectively, were devoid of Galectin 8 (an endosomal damage sensing marker) (Fig. 2A-G). In addition, ~ 70-80% of p97-positive bacteria were not associated with any membrane bound structures (FM4-64 negative) (Fig. 2H, S5). Since, damage to the endosomes by bacterial toxins

generally lead to its cytosolic exposure, mutation in the pneumococcal pore-forming toxin, pneumolysin (Ply), abrogates host ability to mark Δ*ply* variant with p97 (Fig. S2C). However, treatment of cells with LLOMe (Lysomotropic agent) enables it to decorate the Δ*ply* with p97 (Fig. S2B, C), signifying that cytosolic exposure of the bacteria is indispensable for p97's recruitment. Finally, to validate the homing of p97 on the microbial surface, we performed proximity ligation assay using markers such as, enolase (SPN), lipopolysaccharide O antigen (STm), and group A polysaccharide (GAS) and observed significant association of p97 (~ 30-40%) with the intracellular bacteria (Fig. 2I-L). We then examined whether ubiquitination has any role in recruitment of p97 to the pathogen. Treatment of host cells with PYR41, an E1 inhibitor, reduced microbial association of p97 by around 40-70% (Fig. 2M). We further demonstrated that K48-Ub linkages were the primary marker that guides p97 to the target pathogen as 49-57% of the total K48-Ub-associated bacteria recruited p97, while only 18-25% was observed with K63-Ub linkage (Fig. 2N, S6).

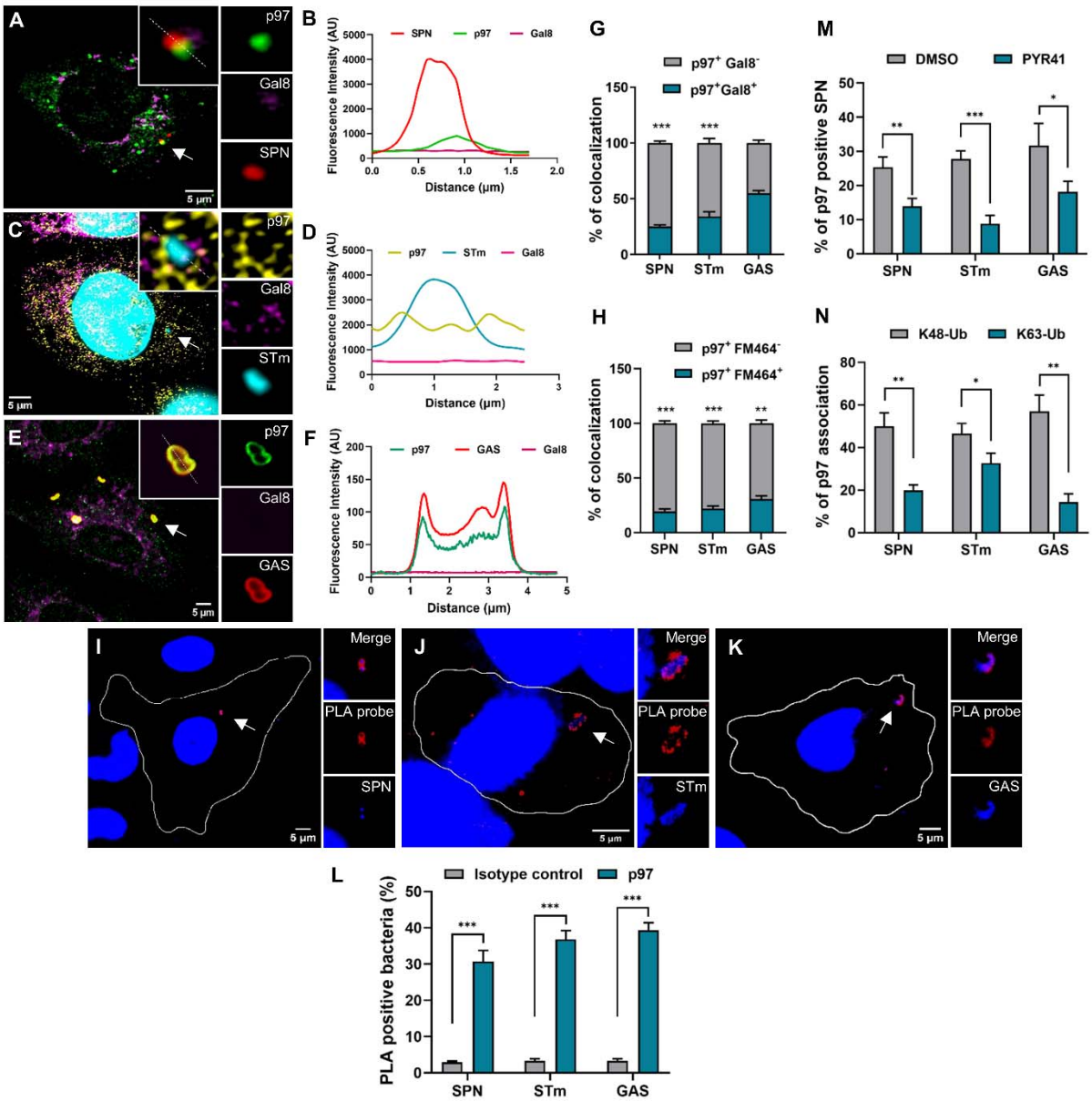

Figure 2. Cytosolic ubiquitinated pathogens are targeted by p97. A,C,E. Structural Illumination Microscopy (SIM) representing the association of p97 (Green or Yellow) with SPN (red) **(A)**, GAS (Red) **(C)** and STm (Cyan) **(E)** devoid of Galectin8 (Magenta). Scale bar, 5 µm. **B,D,F.** Fluorescent line scans across the white dashed line in the merged inset in **(A)**, **(C)** and **(E)**, respectively. **G.** Percentage of cytosolic (Gal8$^-$) or damaged vacuole bound (Gal8$^+$) bacteria marked with p97. n>50 bacteria/coverslip. **H.** Percent association of p97 with cytosolic (FM4-64$^-$) or membrane bound (FM4-64$^+$) bacteria. n>50 bacteria/coverslip. **I-K.** Confocal micrograph showing association of p97 with surface markers of SPN **(I)**, STm **(J)** and GAS **(K)** as determined by Proximity ligation assay (PLA). Scale bar, 5 µm. **L.** Percentage of PLA probe positive bacteria. Isotype control Ab served as a negative control. n>50 bacteria/coverslip. **M.** Quantitative analysis showcasing association of intracellular bacteria with p97 upon treatment with PYR41, an E1 ubiquitin inhibitor,

compared to the control-treated host cells. n>100 bacteria/coverslip. **N.** Percentage of p97-positive bacteria that are decorated with K48-polyUb or K63-polyUb chains. n>100 bacteria/coverslip.
For all immunofluorescence based assays, A549s are infected with SPN and GAS for 9 h while HeLa cells were infected with STm for 6 h. Statistical significance was assessed by two-tailed unpaired student's t-test (nonparametric). *P < 0.05; **P < 0.01; ***P < 0.005. Data are means ± SD of N = 3 independent biological replicates.

VCP/p97 has weak binding affinity towards its ubiquitinated target and requires specific cofactors for efficient association and functioning. K48-Ub recruits NPLOC4 and UFD1 as major cofactors for guiding p97 to the substrate[32]. We therefore evaluated the role of NPLOC4 and UFD1 in bacterial targeting of p97 and found that ~ 68% and 54% of the p97 positive SPN recruited NPLOC4 and UFD1 (Fig. 3A, B), hence confirming their role as primary cofactors in this process. Moreover, ~ 65% of bacteria was dually positive for NPLOC4 and UFD1, indicating their dimeric presence along with p97 on bacterial surface (Fig. 3A). This trimeric association of p97-NPLOC4-UFD1 on ubiquitinated microbial proteins was further substantiated by their co-immunoprecipitation with PspA (Fig. 3C). In addition, knockdown of NPLOC4 and UFD1 (Fig. S3C, D) significantly reduced bacterial association of p97 and consequently doubled intracellular microbial burden (Fig. 3D, E). Since, UFD1 and NPLOC4 bind to the hydrophobic pocket located at the N-terminal region of p97, cells expressing $p97^{\Delta 54\text{-}241}$ variant had diminished (~ 2-fold) targeting of p97 to the pathogen, which resulted in a ~ 1.5-fold increase in the intracellular survival of SPN (Fig. 3F, G, S4D). Overall, these revealed that a coordination between p97, UFD1 and NPLOC4 is vital for targeting cytosol dwelling microbes.

Following extraction by p97, K48-polyubiquitinated bacterial surface proteins should presumably be degraded by proteasomal machinery. Indeed, we found that notable proportions of p97-positive bacteria also recruited proteasomes (represented by proteasomal subunit β7) onto SPN (~ 44%), STm (~ 86%) and GAS (~ 51%) (Fig. S7). Reducing the expression of p97 therefore drastically impeded the association of β7 onto the bacterial surface (Fig. 3H). Additionally, the combination of proteasomal inhibitor (MG132) and p97 depletion elevated intracellular bacterial burden (Fig. 3I), underlining their interplay in guarding the host cytosol (Fig. 3J).

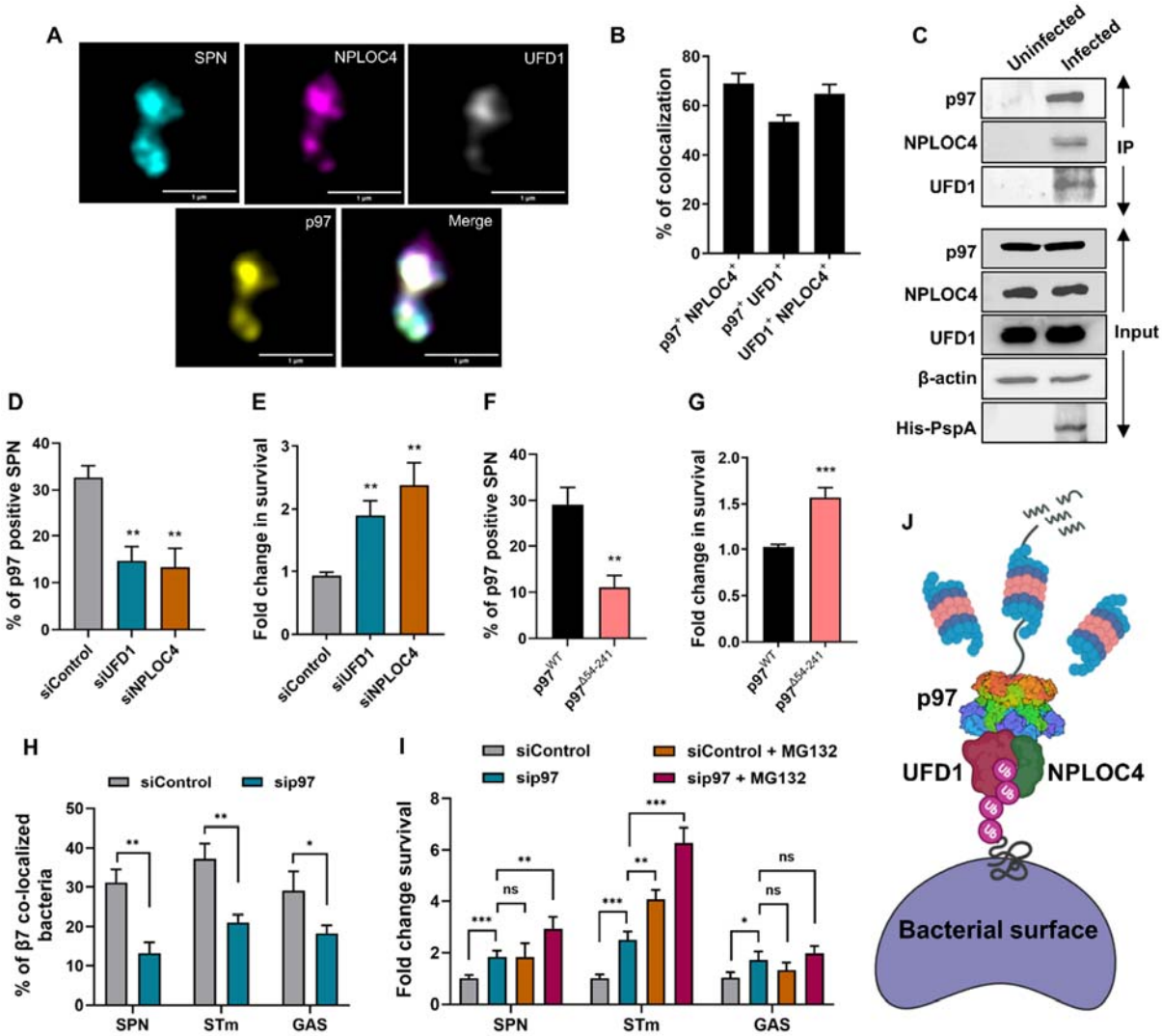

Figure 3. p97 is assisted by NPLOC4, UFD1 and proteasome in clearing bacterial infection. A. Structural Illumination Microscopy (SIM) image depicting association of SPN (Cyan) with p97 (Yellow), UFD1 (Grey), and NPLOC4 (Magenta) following infection of SPN in A549 cells. **B.** Percentage of intracellular SPN associated with either NPLOC4 and p97 or UFD1 and p97 or NPLOC4 and UFD1. n>50 bacteria/coverslip. **C.** Immunoprecipitation of SPN surface protein PspA, displaying its interaction with NPLOC4 and UFD1. **D.** Percentage of intracellular SPN marked with p97 following transfection with siNPLOC4 and siUFD1 compared to siControl. n>100 bacteria/coverslip. **E.** Fold change in intracellular survival of SPN upon treatment of host cells with siNPLOC4 and siUFD1 compared to siControl treated host cells. **F.** Quantitative analysis showcasing association of p97 with intracellular SPN in host cells expressing truncated $p97^{\Delta 54-241}$ compared to wild-type. n>100 bacteria/coverslip. **G.** Fold change in survival of intracellular SPN in host cells expressing truncated $p97^{\Delta 54-241}$ compared to wild-type cells. **H.** Percent association of proteasomal marker β7 with intracellular bacteria in p97 knockdown conditions compared to scramblase (siControl)

treated host cells. n>100 bacteria/coverslip. **I.** Fold change in persistence of intracellular bacteria upon treatment of host cells with either Scramblase control (siControl) or sip97 or siControl + MG132 and sip97 + MG132. **J.** Schematic depicting close co-ordination of p97 with its cofactors NPLOC4 and UFD1 and proteasome while extracting ubiquitinated proteins from bacterial membrane. Scheme was created using Biorender®.

For all immunofluorescence-based assays and intracellular survival assays, A549s are infected with SPN and GAS for 9 h while HeLa cells were infected with STm for 6 h. Statistical significance was assessed by one-way ANOVA followed by Dunnett's test was used for **D, E, I**. Two-tailed unpaired student's t-test (nonparametric) was used for **F, G, H**. *P < 0.05; **P < 0.01; ***P < 0.005. Data are means ± SD of N = 3 independent biological replicates.

Surface protein extraction by VCP/p97 causes deformation in peptidoglycan layer

Since, segregase activity of p97 protects the cytosol from bacterial invasion, we speculated that the mechanical force generated by p97 unfolds its substrate followed by its extraction from bacterial surface. This in turn is postulated to deform the cell-wall integrity. We employed molecular dynamic (MD) simulation in combination with steered MD (SMD), to gain insights into this process. BgaA, a ubiquitinable substrate, was covalently connected to a glycine residue in a pentaglycine bridge present in the peptidoglycan layer at two different levels: (a) outer surface attached and (b) buried (attached to the pentaglycine connected to the second layer of sugar units) (Fig. 4A-C). The ubiquitination site of BgaA, K97, is aligned along the Z-axis since K97-Cα atom will be pulled through the p97 hexamer. Three simulations were performed: (1) Peptidoglycan surface layer devoid of any protein (control); (2) BgaA connected to peptidoglycan surface layer and (3) BgaA connected to the second layer of peptidoglycan. Each of the three realizations were first equilibrated in absence of any external bias. The we performed SMD simulations by pulling BgaA, either surface attached (SMD-S) or buried (SMD-B), through p97 pore, in which the bactoprenol groups are fixed while the K97-Cα atom at the N-terminal of BgaA is being pulled at a constant velocity. The pulling of the K97-Cα atom through the central pore of the p97 hexamer leads to the complete unfolding of BgaA at short time scale followed by subsequent deformation of the peptidoglycan mesh. Till BgaA was unfolded, the force remains stable and fluctuates around 800 pN. Once the protein is completely stretched, there is a steady build-up of force that corresponds to the pulling of the sugar groups of the peptidoglycan from its native integrated configuration, ultimately distorting its mesh-like structure (Fig. 4D, E, Movie S2). To quantify the extent of deformation, we calculated the root-mean-squared-deviation (RMSD) of the peptidoglycan chain containing the sugar units to which BgaA is attached, relative to

its initial undeformed condition. We found that the RMSD values of the peptidoglycan sugar chain closely fluctuates around 6-10 Å in the initial phase in both control and SMD simulations. However, beyond a threshold time, the RMSD of SMD-S and SMD-B simulations gradually increases to a maximum value of 25 Å (Fig. 4F, G). This indicates significant disruption in peptidoglycan during SMD-S and SMD-B compared to the control simulation. Additionally, the extent of distortion was equivalent in both SMD-S and SMD-B, and remained consistent even when pulling velocity was kept low, signifying that as long as the interacting motifs are accessible to the p97, the extraction force would be enough to unfold its substrate and deform the cell wall regardless of its position. These findings hint at a plausible mechanism for the antimicrobial activity of p97, thus motivating us to explore its role in bacterial killing.

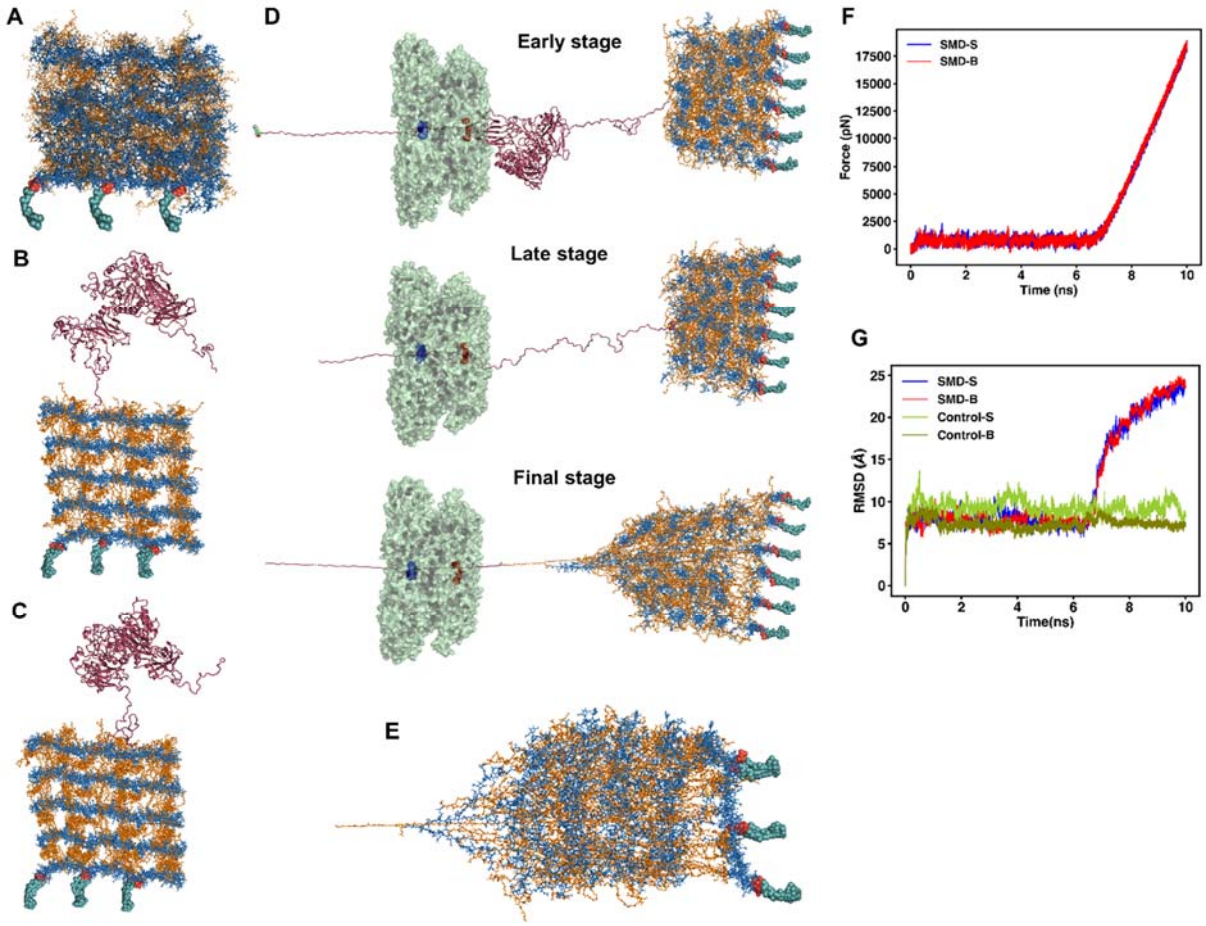

Figure 4. Molecular dynamic simulation of peptidoglycan layer upon extraction of BgaA by p97. A-C. Equilibrated structure of **(A)** Peptidoglycan layer **(B)** BgaA attached on the surface (Control-S) **(C)** BgaA buried in the peptidoglycan mesh (Control-B). **D.** Representative snapshots depicting the early, late, and final pulling simulation of the BgaA-p97-peptidoglycan model (SMD). **E.** Top view of stretched peptidoglycan following p97 mediated pulling of BgaA as shown in "D". **F.** Force extension profile of 10 ns SMD simulation of BgaA pulling (surface and buried, SMD-

S and SMD-B, respectively) through p97 hexamer. **G.** RMSD time evolution of the sugar units of the peptidoglycan mesh connected to BgaA during SMD-S and SMD-B, in comparison to control simulations.

VCP/p97 exhibits bacteriolytic activity

We then focused to unambiguously prove the antimicrobial property of this molecular machine by *in-vitro* reconstitution assay using purified p97, $p97^{E578Q}$, NPLOC4 and UFD1 (Fig. S8A-D). Expectedly, pure p97 exhibited higher ATPase activity compared to $p97^{E578Q}$ variant and its activity further increased following complex formation with NPLOC4 and UFD1 (Fig. S8E-G). To set up the *in-vitro* killing assay, bacteria were pre-ubiquitinated which is necessary for targeting of p97 (Fig. 5A, S9). Remarkably, viabilities of the pathogens were drastically reduced upon incubation with active p97-NPLOC4-UFD1 complex. However, no bacterial killing was observed following treatment with the $p97^{E578Q}$-NPLOC4-UFD1 (Fig. 5B). This confirmed the indispensable role of the ATPase activity associated with the D2 domain and its ability to generate mechanical force for exhibition of bactericidal activity. We also determined the kinetics as well as half inhibitory concentration (IC_{50}) of p97 required in this process (Fig. 5C, D). To prove whether extraction of ubiquitinated proteins by p97 punctures the bacterial membrane, leading to their death, we analysed permeability of Sytox orange (membrane impermeable dye). Indeed, intake of sytox was majorly on p97 positive pathogens (Fig. 5E). Moreover, we found significant increase (~ 4-fold) in sytox positive SPN, STm and GAS population when incubated with active p97 compared to that of denatured or $p97^{E578Q}$ complex (Fig. 5F-H, S10). Further, visualization of bacterial surface morphology by scanning electron microscopy showcased profound rupture or membrane blebbing of all three pathogens while subjected to active p97 treatment (Fig. 5I). We speculate that such large-scale disintegration of the bacterial membrane may lead to release of the internal contents including DNA. Indeed, active p97 triggered excessive leaching of bacterial DNA (~ 2-10-fold) while catalytically inactive or denatured complex showed negligible release (Fig. 5J-L). Together, these results highlight a newly found prominent antimicrobial role of p97 against both Gram-positive and Gram-negative bacteria.

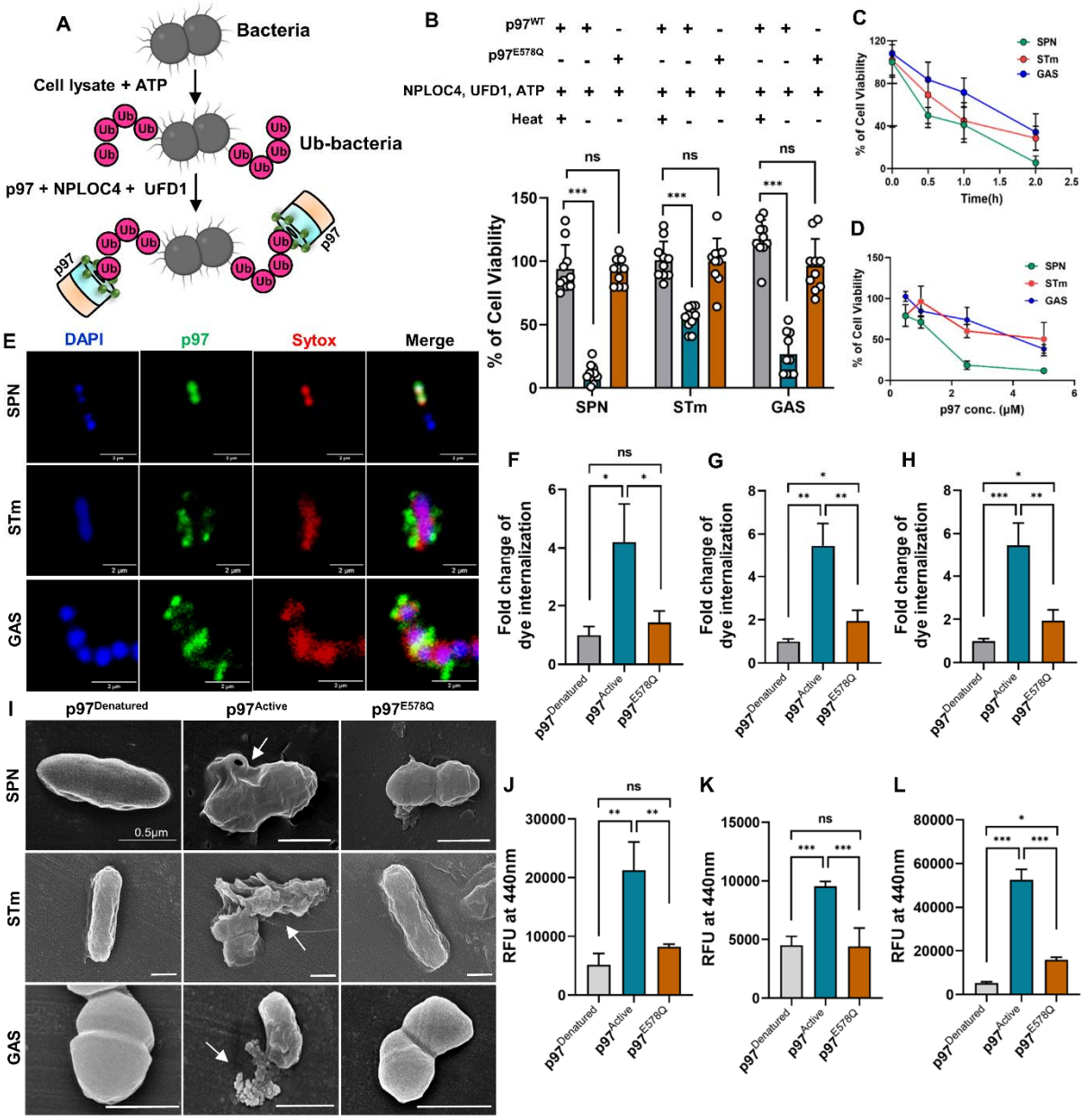

Figure 5. p97 showcases bacteriolytic ability *in-vitro*. A. Schematic representation showing the workflow for *in-vitro* reconstitution of bacterial ubiquitination followed targeting by p97. **B.** Percentage of bacterial cell viability upon treatment with denatured and active p97 complex along with catalytic mutant, $p97^{E578Q}$. **C.** Killing kinetics of p97 complex against various bacteria. **D.** Viability of SPN, STm and GAS following incubation with p97 and co-factors for 2 h over a concentration range (0.5 - 5 μM) to determine the half maximal inhibitory concentration (IC_{50}). **E.** Confocal micrograph showing the internalization of a membrane-impermeable dye, Sytox orange (Red), in bacteria (Blue) upon association with p97 (Green). Bacterial DNA was stained with Hoechst (Blue). **F-H.** Flow cytometry analysis showing the extent of Sytox internalization in SPN **(F)**, STm **(G)** and GAS **(H)** cells following incubation with active p97 complex compared to denatured control and $p97^{E578Q}$. Corresponding

scatter plots depicting percentages of sytox positive bacteria are shown in Fig. S10. n>40000. **I.** Scanning electron microscopy displaying surface disintegration of bacteria upon incubation with active p97 complex, compared to denatured control and $p97^{E578Q}$. Scale bar 0.5 µm. **J-L.** DNA leaching from SPN **(J)**, STm **(K)** and GAS **(L)** upon treatment with active p97 complex compared to denatured control and $p97^{E578Q}$. All experiments were performed with purified proteins. Heat denatured protein complex was used as a negative control. Data are means ± SD of N = 3 independent biological replicates. Statistical significance was assessed by one-way ANOVA followed by Dunnett's test. *P < 0.05; **P < 0.01; ***P < 0.005.

VCP/p97 protects the host from severe bacterial infection

After establishing the critical role of p97 as a bacteriolytic agent, we sought to evaluate its importance as a guarding factor against bacterial infection. Using an established pneumococcus induced *in-vivo* sepsis model (Fig. 6A)[33], we found that inhibition of p97's activity by NMS-873 led to significantly higher mortality of host than vehicle cohort (p=0.0072, log-rank test). While all the p97 inhibited animals succumbed to infection within 38 h, >40% of vehicle treated mice survived during course of the experiment (Fig. 6B). The median survival time (18 h) of the NMS-873 treated mice was considerably lower compared to vehicle cohort (30 h) (Fig. 6B). Moreover, bacterial burden in blood and spleen of the p97 inhibited mice at the time of death was found to be ~ 10-15-fold higher than the vehicle treated animals (Fig. 6C, D). Previous reports suggest that during sepsis, spleen functions as a reservoir for SPN survival and proliferation. At the time of initial rapid clearance of the pathogen from the bloodstream, a minor subset of SPN survives and clonally expand in few splenic macrophages, eventually re-seeding into the blood, causing fatal infection[33]. As inhibiting p97 aggravated the bacterial burden and hampered the host's ability to combat the infection, we speculated that p97 could impede the robust expansion of the pathogen. Indeed, we found that in both spleen and blood, SPN burden kept increasing with time and was ~ 10-12-fold higher in the NMS-873 treated cohort than in the vehicle at 12 h.p.i (Fig. 6E, F). Further, immunohistochemistry studies revealed that splenic burden of SPN in p97 inhibited animals was ~ 4-fold higher and reached as high as 10 bacteria per foci (~ 300 μm^2), in contrast to majorly single SPN in case of vehicle cohort (Fig. 6G-K). Increased bacterial burden, bacterial density in spleen tissues, and number of bacteria per cluster or foci indicate rapid clonal expansion of SPN in absence of immune surveillance by p97. Further, this elevated bacterial burden was found to be associated with increased level of proinflammatory cytokines IL6 and IL-1β in blood and spleen in the p97 inhibited mice compared to vehicle treated group (Fig. 6L, M). These suggest that inhibition of p97 exacerbates pathogen induced septicemia like conditions and demonstrates its utmost importance in host protection against microbial pathogenesis.

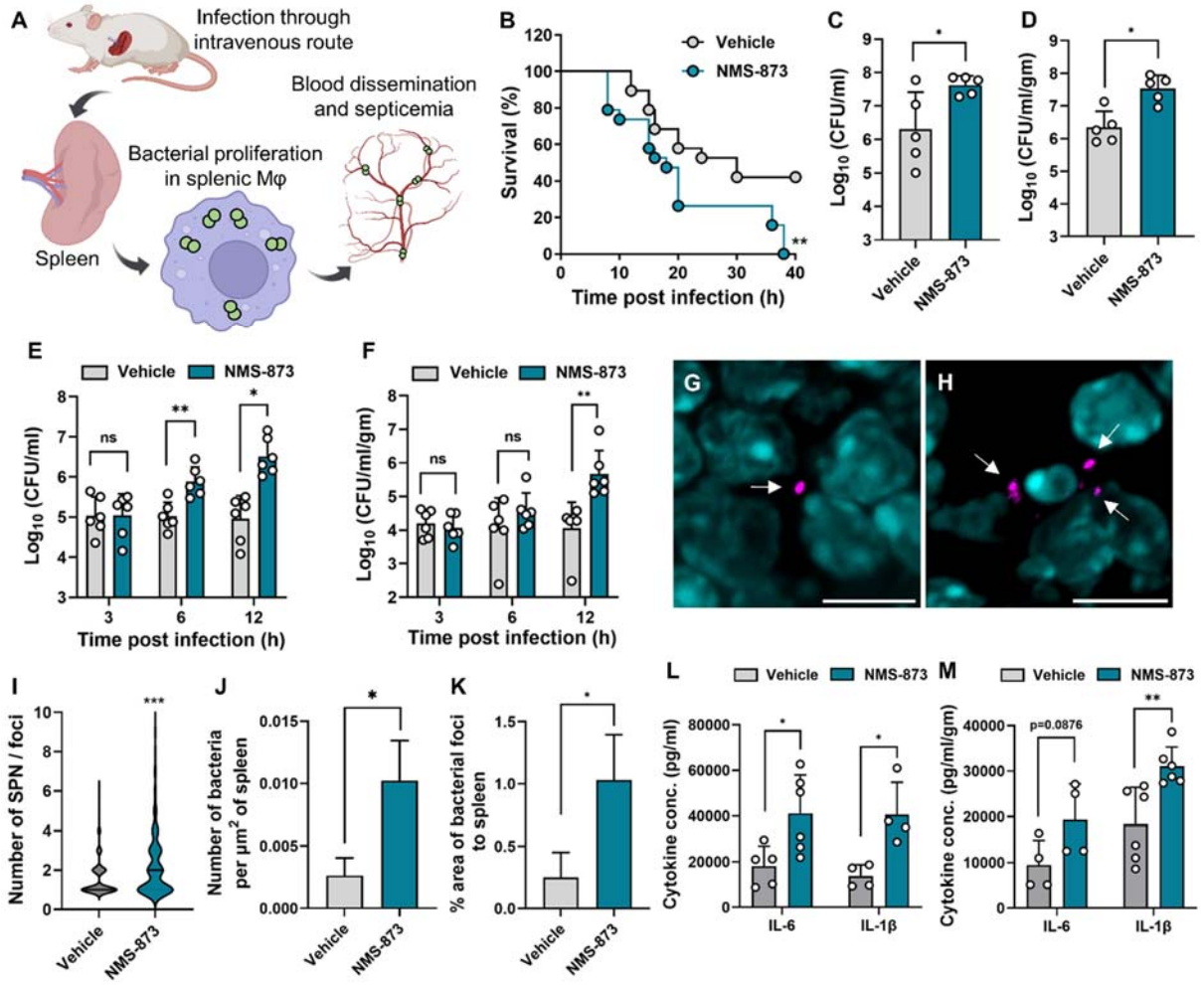

Figure 6. p97 protects mice from bacterial sepsis. A. Schematic describing mouse model of speticemia following pneumococcal infection. **B.** Kaplan-Meier survival curve of mice after i.v. infection with SPN (10^6 CFU) and treatment with either p97 inhibitor NMS-873 or vehicle. n=19 mice per group. **C-D.** Bacterial burden at the time of death in blood **(C)** and spleen **(D)**. n=5 mice per group. **E-F.** Comparison of bacterial burden in blood **(E)** and spleen **(F)** of mice treated with either NMS-873 or vehicle during the first 12 h.p.i with SPN. **G-H.** Representative immunohistochemistry image showing clustering of SPN in spleen of NMS-873 treated mice **(H)** compared to control cohort **(G)**. **I.** Number of SPN per foci, in spleen of animals treated with either NMS-873 or vehicle cohort. **J-K.** Number of bacteria per area (μm^2) of spleen **(J)** and percentage of area occupied by SPN **(K)** in spleen slices from animals treated with NMS-873 compared to vehicle. n=3. **L-M.** Cytokine levels in blood **(L)** and spleen **(M)** at 12 h.p.i. Experiments were repeated twice and data is collectively represented. Statistical analysis was assessed using two-tailed unpaired student's t-test (nonparametric). *P < 0.05; **P < 0.01; ***P < 0.005.

Discussion

Host autonomous immunity has evolved as a consequence of pathogenic challenges. The intent to survive in adversity has driven the development of a gauntlet of efficient immune surveillance systems to detect and defend against all foreign threats. Often invasive pathogens infiltrate host cells and escape lysosomal fusion by modifying the vacuoles harboring them. Accidental or purposeful rupture of such phagosomes leads to release of pathogens into the cytosol. This allows access to nutrients-rich cytosolic environment, which not only could promote microbial growth, but also encourage evasion from vacuolar death traps. However, upon escape into the host cytosol, interferon-induced guanylate binding proteins (GBPs) acts directly on the pathogen's surface which ruptures pathogens and induces pyroptosis[7, 8, 34]. Although the role of GBPs is versatile, its selectiveness to the pathogen's origins, especially towards Gram-negative bacteria, projects an incomplete picture about the diversity and nonspecific nature of the cytoplasmic innate immune mechanisms. This underlines the presence of an unbiased immune sentinel that protects the metazoans against broad-spectrum intruders. Our work unveils a unique bacteriolytic activity of a AAA-ATPase, p97 which harps on diverse cytosol dwelling microbes. By generating mechanical force, these nanomachines extract ubiquitinated substrates common to both Gram-positive and Gram-negative bacteria, leading to their lysis. This unusual generic mechanism employed by the host limits resource diversification and sheds light on a fundamental role of AAA-ATPase family in thwarting microbial infections.

We found that ubiquitin conjugation, mainly K48-polyUb linkage on bacterial surface proteins, is critical for p97's recruitment to microbes. In recent years, ubiquitination has been established as a crucial immune process that senses and tags bacterial pathogens in the host cytosol[4, 19, 28]. The ability of cellular ubiquitination machinery to label a variety of microbes with ubiquitin, drives the impartial bacteriolytic capacity of p97. Naturally, pathogens in their defense also employ an array of secretory ubiquitin ligases and deubiquitinases to either degrade host machinery or modify their surfaces to evade eradication. For example, ubiquitination of GBP1 facilitated by IpaH9.8 neutralizes its activity against *Shigella spp.* infections[34]. Whereas bacterial deubiquitinases such as SseL, deubiquitinates the microbial effectors targeted by the host ubiquitin system[35, 36]. These provide evidence that the pressure of co-existence has driven both host and pathogen to craft innovative strategies to out-manoeuvre each other in the bid for survival and raises the possibility of pathogens utilizing similar strategies to undermine p97's effectiveness.

Typically, p97 extracted proteins from cellular organelles undergo degradation by proteasomes. Along similar lines, we believe that the extracted bacterial surface proteins, when reduced to immunogenic peptides via the proteasomal pathway, have the potential to serve as a source to mount strong cell-mediated immunity through its

association with major histocompatibility complex I. Generally, the 19S AAA-ATPase is closely associated with the proteasome and unfolds substrates before feeding into the 20S proteasomal barrel[37]. Our findings sheds light on the intricate collaboration between p97 and proteasome to tackle cytosolic bacterial population. Notably, the direct interaction between p97 and SPN surface protein PspA, suggest the significant role of p97 in protein unfolding, particularly in the context of surface-bound substrates, while the activity of proteasomal unfoldase (PSMC6) was not prominent. In addition, bacterial clearance due to the combination of both p97 and proteasome was found to be pronounced for STm compared to SPN and GAS. This could be attributed to proteasomal degradation of STm effector proteins such as SopE and SptP, which play crucial part in its survival and replication[38, 39]. On the contrary, a previous report demonstrate passive participation of p97 in antibody-dependent intracellular neutralization of viral particles[40]. However, our findings redefine the role of p97-proteasomal axis as a robust innate immune surveillance tactic in dispelling bacterial infections independent of adaptive immunity.

VCP/p97 has diverse cellular roles, however, its function and targeting are tightly controlled by specific cofactors. Ubiquitin binding domain carrying cofactors such as NPLOC4 and UFD1 recognizes K48-polyUb linkages on the pathogen. The UBXL and SHP motif of NPLOC4 and UFD1, respectively, binds to the two hydrophobic non-competing crevices located in the N-terminal region of p97 and plays a significant role in directing the AAA-ATPase towards the threat[41]. Although, we acknowledge the existence of multiple cofactors carrying ubiquitin binding domain to be associated with p97, our results identified these two cofactors exhibiting a dominant effect in modulating p97's antibacterial activity. This suggests that combination of various pathways inflicted by the host is paramount in resisting bacterial invasion and regulation of such mechanism is well-orchestrated to avoid non-specific conflicts.

Invasive pathogens often establish systemic infections by replicating in splenic macrophages from where they re-seed into the circulatory system to overwhelm the host[33]. While CD169+ splenic macrophages are known to have ineffective antiviral and bactericidal responses due its un-responsiveness to type I IFN signalling[33, 42], the pathogenic burden generated in them contribute significantly in antigen presentation followed by activation of adaptive immunity[43]. However, the subdued type I interferon response known to hamper cell-autonomous immunity including the innate degradative machinery in such macrophages[44]. This could be the underlining cause for the immunocompromised nature of such sites, thereby highlighting the potential role of cytosolic guarding factors in averting proliferation in general APCs (antigen presenting cells) or other cell types. Interestingly, our results emphasize a key role of p97 in impeding bacterial replication in the spleen and their dissemination into the vasculature. Furthermore, depriving the host of p97 instigates a devastating cytokine storm culminating in a fatal outcome, thereby illustrating its indispensable nature in

ensuring host survival. We further postulated that mutations in p97 leading to inept functioning might be a detrimental blow to microbial clearance. In fact, patients carrying such mutations suffer from inclusion body myopathy with early onset of Paget disease and frontotemporal dementia (IBMPFD) and notably linked to disruption of various homeostasis processes, including lysosomal storage and organellar recycling[45]. Remarkably, we observed a striking relation between host cells expressing such hotspot mutations of p97 with profound inability to clear pathogens, leading to escalated infection susceptibility. This correlation between polymorphism in individuals and their vulnerability to infections has also been noted in patients afflicted with Parkinson's and chronic lymphocytic leukemia (CLL)[19, 20]. Collectively, these serve as a strong reminder that genetic makeup of individuals can influence the on-going battle against pathogenic adversaries and have a cardinal impact on innate defense.

In conclusion, we unravel an ancient yet powerful class of host immune factor that plays a decisive role in clearance of diverse pathogenic bacteria. Exploitation of such broad-spectrum antimicrobial mechanism could tip the balance in favour of the host against ever evolving bacterial and non-bacterial foes.

Materials and Methods

Antibodies and Reagents

Antibodies against VCP/p97 (MA3-004), NPLOC4 (PA554749), PSMB7 (PA5-111404), PSMC6 (PA5-60140), β-Actin (MA5-15739), Group A *Streptococcus* (PA1-73059), MDN1 (PA5-56225) were purchased from ThermoFisher Scientific. Antibodies specific for UFD1 (Santa Cruz Biotechnology, sc-377265), K48-Ub linkage (MERCK, 05-1307), Phosphothreonine (Cell Signaling, Technology 9381S), K63-Ub linkage (Enzo, BMLBML-PW0600-025), *Salmonella* O antisera (Difco, 225341), Anti-Enolase (Prof. S. Hammerschmidt, University of Greifswald, Germany), VPS4 (MERCK MABC83) were used in the study. HRP tagged anti-rabbit (Biolegend 406401), HRP tagged anti-mouse (Biolegend, 405306), anti-rabbit Alexa Fluor 555 (Invitrogen, A31572), Anti-rabbit Alexa Fluor 488 (Invitrogen, A27206), anti-mouse Alexa Fluor (Invitrogen, A31570), anti-goat Alexa Fluor 633 (Invitrogen, A21082), anti-mouse Alexa Fluor 488 (Invitrogen, A21202), Biotin conjugated anti-mouse IgaA (Life Tech., M31115), were used as secondary antibody.
Pharmacological inhibitors and small molecule reagents such as DBeQ (SML0031), NMS-873 (SML1128), PYR41 (N2915), and LLOMe (L1002) were purchased from MERCK. Dyes such as FM4™-64 (T3166) and SYTOX™ Orange Dead Cell Stain for flow cytometry (S34861) were purchased from ThermoFisher Scientific.

Cell culture and Transfection

Human lung alveolar carcinoma (type II pneumocyte) cell line A549 (ATCC No. CCL-185) and cervical adenocarcinoma cell line HeLa (ATCC No. CRM-CCL-2) were grown in DMEM (HiMedia, AT007) which was supplemented with 10% FBS (GIBCO, 38220090) at 5% CO_2 at 37°C. Transfections were performed using Lipofectamine 3000 (ThermoFisher Scientific, L3000001) according to the manufacturer's protocol, and selections were done in the presence of 2 µg/ml blasticidin hydrochloride (HiMedia, TC421).

Bacterial Strains and Growth Conditions

E. coli (DH5α, BL21(DE3), Rosetta (DE3)) cultures and *Salmonella enterica* Serovar Typhimurium (STm) (ATCC 14028) were grown in Luria-Bertani broth (LB) at 37°C under shaking conditions (200 rpm). *Streptococcus pneumoniae* (SPN) strains R6 (serotype 2, unencapsulated) and D39 (serotype 2, capsulated) (provided by Prof. TJ Mitchell, Univ. of Birmingham, UK) and *Streptococcus pyogenes* (GAS) strain JRS4 (obtained from Prof. Victor Nizet, Univ. of California-San Diego, USA) were grown at 37°C with 5% CO_2 in Todd-Hewitt broth (THB) supplemented with 1.5% yeast extract. Following antibiotics were used when required: ampicillin (100 µg/ml, for *E. coli*), kanamycin (50 µg/ml for *E. coli* and 200 µg/ml for SPN), chloramphenicol (20 µg/ml for *E. coli* and 4.5 µg/ml for SPN) and spectinomycin (100 µg/ml for SPN).

Gentamicin protection assay

SPN, STm and GAS grown till OD_{600nm} 0.4 were used to infect monolayers of A549s (with SPN at MOI ~ 10 and GAS at MOI ~ 2) or HeLa (with STm at MOI ~ 50) for 1 h. After washing, extracellular bacteria were killed using antibiotics (10 µg/ml penicillin and 400 µg/ml gentamicin for SPN or 200 µg/ml gentamicin for STm and GAS) for 2 h. Following washes with 1X PBS, cells were trypsinized (0.025% trypsin EDTA), lysed (0.025% Triton X-100), and serial dilutions of the lysates were plated on Brain Heart Infusion (BHI) agar plates to enumerate bacterial colonies. Bacterial invasion efficiency was calculated as (recovered CFU/initial inoculum CFU) × 100%. To calculate the intracellular survival of the bacteria, infected cell lysates at different time points were spread-plated, enumerated, and represented as percent survival at indicated time points relative to 0 h (post-antibiotic treatment). The ratio of survival efficiencies of the test to that of control was calculated and represented as fold change survival

Fluorescence Microscopy

A549 and Hela cells grown on glass coverslips were infected with SPN (MOI ~ 25), GAS (MOI ~ 2), and STm (MOI ~ 50). At desired time points post-infection, cells were washed with 1X PBS, and fixed with ice-chilled Methanol for 10 min at -20°C. Further, 3% BSA was used for blocking for 2 h at RT. Cells were then treated with the appropriate primary antibody in 1% BSA overnight at 4ºC, followed by incubation with a suitable secondary antibody in 1% BSA for 1 h at RT. Finally, coverslips were washed with PBS and mounted on glass slides along with VectaShield® with or without DAPI (Vector Laboratories) for visualization using a Laser Scanning Confocal microscope (Carl Zeiss LSM 780) under 40X or 63X oil objective or using Nikon AXR microscope for Instant-Structured Illumination Microscopy (iSIM) at a 60X or 100X oil objective. The images were acquired after optical sectioning and then processed using Zen lite software (Version 5.0.).
For time-lapse microscopy, A549 cells were grown on a 35 mm glass bottom petridish, followed by infection with SPN. Time-lapse imaging was performed in Zeiss observer Z1 with optical sectioning under 63X oil objective.

Proximity Ligation Assay

For *ex-vivo* proximity ligation, SPN infected A549s were fixed with chilled methanol followed by further processing with Duolink® In Situ Orange Starter Kit Mouse/Rabbit (MERCK, DUO92102-IKT) according to the manufacturer's protocol. Fixed cells were imaged as mentioned above and the colocalization events were quantified using Zen Blue 3.7.

Transmission electron microscopy

Following infection of A549 and Hela cells with SPN, GAS and STm, respectively, cells were washed with 0.1 M sodium cacodylate buffer, fixed with 2% paraformaldehyde and 0.5% glutaraldehyde in 0.1 M phosphate buffer, pH 7.4 at room temperature for 2 h. Cells were then washed thoroughly, collected through a cell scraper, and pelleted at 2000 rpm for 10 min. Gradually dehydration was performed with gradient of ethanol (50%, 70%, 90%, and 100% for 15 min), followed by infiltration in ethanol and LR white resin mixtures at 1:1 and embedding in pure LR white resin (Electron Microscopy Sciences, 14300) by polymerization at 65°C for 24 to 48 h. Ultrathin sections (70 nm) were cut using a diamond knife on a Leica EM UC7 Ultramicrotome. The grids were transferred onto drops of the matching Aurion-blocking solution for 15 min and washed with PBS followed by incubation with 1:50 of p97 primary and 25 nm gold conjugated secondary antibody for 1 h at room temperature. The grids were contrasted with uranyl acetate for 15 min and sections were viewed using a transmission electron microscope (Talos L120 C, Thermo Fisher Scientific) at 120 kV.

Vector constructs

For transfection, EGFP-p97 gene was amplified from pEGFP-p97 (Addgene #85670) and cloned into pMRX vector (Gifted by T Yoshimori, Osaka University, Japan). Further site directed mutagenesis was performed to create various p97 variants (E578Q, ∆54-241, L198W and R155H) in the pMRX background (Table S2, S3).
For protein purification, p97 gene was amplified from pMRX-EGFP-p97 and cloned into pET28a vector along with $p97^{E578Q}$ variant which was further transformed into *E. coli* BL21(DE3). We added 6X-His at the C-terminal end of NPLOC4 and cloned into pET41b followed by transformation into Rosetta (DE3). (Table S2, S3).

Protein expression and purification

E. coli Bl21(DE3) strain carrying p97 or p97 (pAB713 and pAB730, respectively) or *E. coli* Rosetta(DE3) harbouring NPLOC4 and UFD1 (pAB720 and Addgene #117107, respectively) were cultured in LB as described above. The overnight cultures were re-suspended in fresh LB (1:10) and were incubated at 37°C. At OD_{600nm} ~ 0.8, isopropyl-1-thiogalactopyranoside (IPTG) (200 µM for p97 and its variants, 1 mM for NPLOC4 and UFD1, respectively) was added to the cultures, followed by further incubation for 5 h at 37°C. For NPLOC4 expression, post IPTG addition cultures were further incubated at 18°C for 16 h. The bacterial suspensions were pelleted down at 4000 rpm for 15 min and re-suspended in lysis buffer (50 mM Tris-Cl, 300 mM NaCl, 5 mM β-mercaptoethanol, 1 mM PMSF, 5% glycerol, pH.8) and lysed by sonication. The sonicated lysates were centrifuged at 15000 rpm for 30 min and the supernatants collected were loaded onto the equilibrated Ni-NTA column. Columns were washed with buffer (50 mM Tris-Cl, 300 mM NaCl, 5 mM β-mercaptoethanol, 5% Glycerol) containing 30 µM imidazole and bound proteins were with 250 µM imidazole. The eluted fractions were pulled, concentrated with Amicon ultrafiltration unit (10 kDa) and buffer exchanged in 200 mM HEPES, 1 M KCl, 100 mM $MgCl_2$, pH 7.4, using PD-10 columns (GE Healthcare).

Western blotting

Mammalian cells were lysed in ice-cold RIPA buffer (50 mM Tris-Cl, pH 7.89, 150 mM NaCl, 1% Triton X-100, 0.5% Sodium deoyxycholate, 1% SDS) containing protease inhibitor cocktail (Promega), Sodium fluoride (10 mM) and EDTA (5 mM). Protein was estimated using Bradford reagent (ThermoFischer Scientific), separated on 8-12% SDS-PAGE gels after adding the Laemmli SDS loading buffer and transferred to activated PVDF or nitrocellulose membrane. Finally, the membrane was blocked with 5% skimmed milk and probed with appropriate primary and secondary HRP-conjugated antibodies. Visualization of the blots was done using ECL substrate (Bio-Rad) using a Chemidoc (BioRad).

Immunoprecipitation

SPN expressing PspA-$(His)_6$ was infected into host cells (A549) followed by cellular lysis using RIPA buffer after 9 h post infection. Equal amounts of lysate of infected and non-infected cells were incubated with 5 µg of anti-$(His)_6$ antibody overnight at 4˚C. 40 µl of Protein G Sepharose® was added to the lysate and incubated for 3 h at 4˚C. The beads were then centrifuged at 7000 rpm for 3 min and washed thoroughly. Finally, the sample was separated in SDS-PAGE after addition of Laemmli SDS loading buffer and transferred onto the PVDF membrane followed by probing with specific antibodies for visualization under Chemidoc (BioRad).

ATPase assay

The ATPase activity of p97 was measured using the Malachite Green Phosphate assay kit (Sigma, MAK307) according to the manufacturer's protocol in a reaction buffer containing 200 mM HEPES, 1 M KCl, 100 mM $MgCl_2$, and 10 µM ATP, pH 7.4. Absorbance was measured at 620nm and normalized to 0 h and the turnover of free phosphate was calculated.

In-vitro ubiquitination assay

In-vitro ubiquitination was performed by incubating bacteria with host cell lysate. A549 cell lysate was prepared by scraping the cells from T75 flasks at 4°C, followed by sonication (amplitude 40 mA; 2-sec on followed by 2-sec off) in reaction storage buffer (200 mM HEPES, 1 M KCl, 100 mM $MgCl_2$, and 5% Glycerol, pH 7.4). The supernatant was collected from the sonicated product by centrifuging at 15000 rpm for 45 min, followed by flash freezing (in liquid nitrogen).
100 µl of mid-exponentially grown SPN (approximately 10^8 cells/ml) was centrifuged, and the pellet was incubated with A549 cell lysate (2 mg/ml total protein) along with 1 mM ATP for 1-2 h at room temperature. The bacteria were washed three times with the reaction buffer containing 3 M urea and ubiquitination of bacteria was analysed by western blotting with anti-K48-Ub Ab.

In-vitro killing assay

Purified p97 (5 µM), NPLOC4, and UFD1 were mixed in a 6:1:1 ratio and incubated on ice for 3 h in a buffer containing 200 mM HEPES, 1 M KCl, 100 mM $MgCl_2$, 5% glycerol and 1 mM ATP (reaction buffer). Ubiquitinated bacteria were incubated for 1-2 h with the p97 complex at 37°C, followed by colony enumeration on BHI or LA plates compared to denatured control normalized with 0 h.

Scanning electron microscopy

Ubiquitinated SPN, STm and GAS were incubated with p97-UFD1-NPLOC4 complex for 1h. Bacterial cells were then fixed with 2.5% glutaraldehyde for 3 h at room temperature, followed by repeated washing with distilled water. The samples were serially dehydrated with 10%, 30%, 50%, 70%, and 100% ethanol, spotted and air dried on an aluminium tray followed by imaging via (Field emission gun) FEG-SEM (JSM 7600F).

In-vitro DNA release

Ubiquitinated bacteria were incubated with Hoechst 33342 (5 µg/ml) (ThermoFisher Scientific) for 10 min to stain the DNA. Stained bacterial suspension was mixed with VCP/p97 complex and incubated for 2 h at 37°C. Post incubation, bacterial suspensions were centrifuged and relative fluorescence unit (RFU) of the supernatants collected were determined by a spectrofluorimeter with an excitation wavelength of 360 nm and emission at 440 nm.

Flow Cytometry

After treatment of ubiquitinated bacteria (10^7) with p97 complex, cells were washed with 1X PBS followed by incubation with SYTOX™ Orange Dead Cell Stain (ThermoFisher Scientific) for 20 min according to the manufacturer's protocol. Flow cytometry was performed using a BD FACS Aria-Fusion flow cytometer with at least 30000 events to detect Sytox positive bacteria with an emission wavelength of 561nm. For analysis, FlowJo (Version 9.3) was used.

RNA interference

For siRNA-mediated gene knockdown, ON-TARGET PLUS SMARTpool specific for VCP/p97 (L-008727-00-0010, 15pmol), UFD1 (L-017918-00-0005, 10pmol), NPLOC4 (L-020796-01-0005, 15pmol) and PSMC6 (L-009570-01-0005, 15pmol) were purchased from Dharmacon. A549 and Hela cells were plated in a 24-well plate followed by appropriate siRNA transfection using Lipofectamine RNAiMAX (ThermoFischer Scientific) according to the manufacturer's protocol.

In-vivo sepsis model

All the experimental work on animals were done as per the guidelines of the Committee for the Purpose of Control and Supervision of Experiments on Animals (CPCSEA), India. The study protocol has been reviewed and approved by the Institutional Animal Ethics Committee (IAEC, Reg. no. 48/1999/CPCSEA) of Indian

Institute of Science (IISc, Bengaluru, India) under the project number CAF/Ethics/380/2014. Briefly, 6-8 weeks old CD1 female mice with an average weight of 20 to 24 gm were injected intravenously via tail-vein injection with 10^6 SPN. In two different cohorts, animals were treated intra-peritoneally with either DMSO (vehicle) or p97 inhibitor, NMS-873. Mice were culled when they were moribund or at specific time points. Blood samples were obtained by cardiac puncture and excised spleens were processed via a handheld homogenizer. For enumeration of bacterial burden, blood and spleen homogenates were serially diluted and then plated on sheep blood agar plates which were incubated overnight at 37°C, 5% CO_2, and bacterial colony numbers were assessed the following day.

ELISA

Cytokine levels in the serum and spleen of mice infected with *SPN* were measured using ELISA MAX™ Standard Set Mouse IL-6 (BioLegend 431301) and ELISA MAX™ Standard Set Mouse IL-1β (BioLegend 432601) according to the manufacturer's protocol.

Immunohistochemistry

Spleens were fixed in 4% paraformaldehyde, embedded in paraffin and 5 µm thick paraffin sections were collected on poly-lysine coated glass slides. Tissue sections were incubated in 100% Xylene for 20 min, followed by washing in 1X PBS with 0.05% tween 20. Staining was performed with anti-enolase Ab (specific for SPN, provided by Pro. Sven Hammarschmidt, Univ. of Greifswald, Germany; 1:5000) followed by AlexaFluor-488 conjugated secondary Ab (1:100). Sections were then washed with 1X PBS, mounted using Vecta-shield with DAPI (Vector Laboratories) and visualized under a Laser Scanning Confocal microscope (Carl Zeiss LSM 780).

Molecular Dynamics Simulation

Molecular dynamics (MD) simulation was used to model the disruption of the structural integrity of bacterial peptidoglycan upon extraction of the ubiquitinated bacterial surface protein, BgaA, through the pore of the host p97 hexamer. The structure of the human p97 hexamer was derived from protein database (PDB ID: 7BP8)[46] and structure of truncated version (97-1036 a.a.) of BgaA, was predicted using AlphaFold2[47]. Adopting an all-atom model of *Staphylococcus aureus* peptidoglycan[48], we built a 3D peptidoglycan mesh consisting of 6 x 5 chains of peptidoglycan crosslinked by pentaglycine chains. We performed implicit solvent simulations of the system using the generalized Born implicit solvent model as implemented in NAMD 2.14 and performed at a timestep of 1 fs. The CHARMM36m force field is used for the proteins BgaA and p97[49]. An α cutoff, corresponding to the Born radius of the atoms

is set as 12 Å. The nonbonded Lennard Jones interactions are cut off at a distance of 14 Å with a switching function at 13 Å. The system temperature is maintained at 310 K using a Langevin thermostat.

In order to simulate the process of extraction of BgaA through the pore of p97 hexamer, we harnessed the technique of steered MD simulations, which is an enhanced sampling technique for sampling rare events. SMD simulations were performed with the bactoprenol groups fixed and the Cα atom of K97 in BgaA subjected to pulling at constant velocity. The simulation time scale was 1 ns and 10-12 ns using pulling velocities of 0.005 Å/timestep (equivalent to 5 Å/ps) and 0.0005 Å/timestep (equivalent to 0.5 Å/ps). Visualization and analyses of the simulation were performed using VMD[7] and TCL scripting interface.

Statistical analysis

Statistical analyses were performed using GraphPad Prism software (version 9). Statistical tests undertaken for individual experiments are mentioned in the respective figure legends. Statistical significance was accepted at $p<0.05$. All multi-parameter analyses included corrections for multiple comparisons, and data are presented as means ± SD unless otherwise stated.

Acknowledgements

We acknowledge the "Bio-safety Level 2 Facility" and “Confocal Microscopy Facility” at IIT Bombay. We also acknowledge Electron microscopy facility at CSIR-CCMB, Hyderabad, India, and Animal facility at IISc, Bengaluru, India.

Funding

SG, DH and SR, SRa acknowledges fellowship from CSIR and UGC, Govt. of India, respectively. SS acknowledges fellowship from PMRF, Govt. of India. AB acknowledges research funding from Science and Engineering Research Board, Govt. of India (Grant No. SPR/2019/000808) and Ignite Life Science Foundation (Grant No. IGNITE/FG-OC/2021/004). The funders had no role in study design, data collection and analysis, decision to publish, or preparation of the manuscript.

Author contributions

Conceptualization: AB
Methodology: SG, SR, NB, UKD, DH, SM, MS, HA
Validation: SG, SR, NB, UKD, DH, SM, MS
Formal Analysis: SG, SR, DH, SM, MS, JM, AB
Investigation: SG, SR, NB, UKD, DH, SM, MS, SS, Sra, RSR, HA
Resources: JM, DC, AB
Data Curation: SG, SR, JM, AB
Writing – Original Draft Preparation: SG, AB
Writing – Review & Editing Preparation: SG, NB, SR, SS, AB
Visualization: SG, SR, NB
Supervision: JM, DC, AB
Project Administration: AB
Funding Acquisition: AB

Competing interests: Authors declare no competing interests.

References

1. Mogensen, T.H. Pathogen recognition and inflammatory signaling in innate immune defenses. *Clin Microbiol Rev* **22**, 240-273, Table of Contents (2009).

2. Zindel, J. & Kubes, P. DAMPs, PAMPs, and LAMPs in Immunity and Sterile Inflammation. *Annu Rev Pathol* **15**, 493-518 (2020).

3. Bee, G.C.W. *et al.* Age-dependent differences in efferocytosis determine the outcome of opsonophagocytic protection from invasive pathogens. *Immunity* (2023).

4. Thurston, T.L., Wandel, M.P., von Muhlinen, N., Foeglein, A. & Randow, F. Galectin 8 targets damaged vesicles for autophagy to defend cells against bacterial invasion. *Nature* **482**, 414-418 (2012).

5. Shenoy, A.R. *et al.* Emerging themes in IFN-gamma-induced macrophage immunity by the p47 and p65 GTPase families. *Immunobiology* **212**, 771-784 (2007).

6. Rafeld, H.L., Kolanus, W., van Driel, I.R. & Hartland, E.L. Interferon-induced GTPases orchestrate host cell-autonomous defence against bacterial pathogens. *Biochem Soc Trans* **49**, 1287-1297 (2021).

7. Feng, S. *et al.* Pathogen-selective killing by guanylate-binding proteins as a molecular mechanism leading to inflammasome signaling. *Nat Commun* **13**, 4395 (2022).

8. Wandel, M.P. *et al.* Guanylate-binding proteins convert cytosolic bacteria into caspase-4 signaling platforms. *Nat Immunol* **21**, 880-891 (2020).

9. Gaudet, R.G. *et al.* A human apolipoprotein L with detergent-like activity kills intracellular pathogens. *Science* **373** (2021).

10. MacMicking, J.D. Interferon-inducible effector mechanisms in cell-autonomous immunity. *Nat Rev Immunol* **12**, 367-382 (2012).

11. Ellison, C.J., Kukulski, W., Boyle, K.B., Munro, S. & Randow, F. Transbilayer Movement of Sphingomyelin Precedes Catastrophic Breakage of Enterobacteria-Containing Vacuoles. *Curr Biol* **30**, 2974-2983 e2976 (2020).

12. Surve, M.V. *et al.* Heterogeneity in pneumolysin expression governs the fate of Streptococcus pneumoniae during blood-brain barrier trafficking. *PLoS Pathog* **14**, e1007168 (2018).

13. Deol, K.K., Lorenz, S. & Strieter, E.R. Enzymatic Logic of Ubiquitin Chain Assembly. *Front Physiol* **10**, 835 (2019).

14. Otten, E.G. *et al.* Ubiquitylation of lipopolysaccharide by RNF213 during bacterial infection. *Nature* **594**, 111-116 (2021).

15. Yamada, A., Hikichi, M., Nozawa, T. & Nakagawa, I. FBXO2/SCF ubiquitin ligase complex directs xenophagy through recognizing bacterial surface glycan. *EMBO Rep* **22**, e52584 (2021).

16. Chauhan, S. *et al.* TRIMs and Galectins Globally Cooperate and TRIM16 and Galectin-3 Co-direct Autophagy in Endomembrane Damage Homeostasis. *Dev Cell* **39**, 13-27 (2016).

17. Ogawa, M. *et al.* Molecular mechanisms of Streptococcus pneumoniae-targeted autophagy via pneumolysin, Golgi-resident Rab41, and Nedd4-1-mediated K63-linked ubiquitination. *Cell Microbiol* **20**, e12846 (2018).

18. Noad, J. *et al.* LUBAC-synthesized linear ubiquitin chains restrict cytosol-invading bacteria by activating autophagy and NF-kappaB. *Nat Microbiol* **2**, 17063 (2017).

19. Manzanillo, P.S. *et al.* The ubiquitin ligase parkin mediates resistance to intracellular pathogens. *Nature* **501**, 512-516 (2013).

20. Apte, S. *et al.* An innate pathogen sensing strategy involving ubiquitination of bacterial surface proteins. *Sci Adv* **9**, eade1851 (2023).

21. Nickell, S. *et al.* Insights into the molecular architecture of the 26S proteasome. *Proc Natl Acad Sci U S A* **106**, 11943-11947 (2009).

22. van den Boom, J. & Meyer, H. VCP/p97-Mediated Unfolding as a Principle in Protein Homeostasis and Signaling. *Mol Cell* **69**, 182-194 (2018).

23. Kim, Y.C., Snoberger, A., Schupp, J. & Smith, D.M. ATP binding to neighbouring subunits and intersubunit allosteric coupling underlie proteasomal ATPase function. *Nat Commun* **6**, 8520 (2015).

24. Erzberger, J.P., Mott, M.L. & Berger, J.M. Structural basis for ATP-dependent DnaA assembly and replication-origin remodeling. *Nat Struct Mol Biol* **13**, 676-683 (2006).

25. Story, R.M. & Steitz, T.A. Structure of the recA protein-ADP complex. *Nature* **355**, 374-376 (1992).

26. Khan, Y.A., White, K.I. & Brunger, A.T. The AAA+ superfamily: a review of the structural and mechanistic principles of these molecular machines. *Crit Rev Biochem Mol Biol* **57**, 156-187 (2022).

27. Bhutda, S. *et al.* Differential Ubiquitination as an Effective Strategy Employed by the Blood-Brain Barrier for Prevention of Bacterial Transcytosis. *J Bacteriol* **204**, e0045621 (2022).

28. Franco, L.H. *et al.* The Ubiquitin Ligase Smurf1 Functions in Selective Autophagy of Mycobacterium tuberculosis and Anti-tuberculous Host Defense. *Cell Host Microbe* **22**, 421-423 (2017).

29. Iovino, F., Gradstedt, H. & Bijlsma, J.J. The proteasome-ubiquitin system is required for efficient killing of intracellular Streptococcus pneumoniae by brain endothelial cells. *mBio* **5**, e00984-00914 (2014).

30. DeLaBarre, B., Christianson, J.C., Kopito, R.R. & Brunger, A.T. Central pore residues mediate the p97/VCP activity required for ERAD. *Mol Cell* **22**, 451-462 (2006).

31. Zhang, X. *et al.* Altered cofactor regulation with disease-associated p97/VCP mutations. *Proc Natl Acad Sci U S A* **112**, E1705-1714 (2015).

32. Ye, Y., Meyer, H.H. & Rapoport, T.A. Function of the p97-Ufd1-Npl4 complex in retrotranslocation from the ER to the cytosol: dual recognition of nonubiquitinated polypeptide segments and polyubiquitin chains. *J Cell Biol* **162**, 71-84 (2003).

33. Ercoli, G. *et al.* Intracellular replication of Streptococcus pneumoniae inside splenic macrophages serves as a reservoir for septicaemia. *Nat Microbiol* **3**, 600-610 (2018).

34. Li, P. *et al.* Ubiquitination and degradation of GBPs by a Shigella effector to suppress host defence. *Nature* **551**, 378-383 (2017).

35. Mesquita, F.S. *et al.* The Salmonella deubiquitinase SseL inhibits selective autophagy of cytosolic aggregates. *PLoS Pathog* **8**, e1002743 (2012).

36. Rytkonen, A. *et al.* SseL, a Salmonella deubiquitinase required for macrophage killing and virulence. *Proc Natl Acad Sci U S A* **104**, 3502-3507 (2007).

37. Tomita, T. & Matouschek, A. Substrate selection by the proteasome through initiation regions. *Protein Sci* **28**, 1222-1232 (2019).

38. Vonaesch, P. *et al.* The Salmonella Typhimurium effector protein SopE transiently localizes to the early SCV and contributes to intracellular replication. *Cell Microbiol* **16**, 1723-1735 (2014).

39. Kubori, T. & Galan, J.E. Temporal regulation of salmonella virulence effector function by proteasome-dependent protein degradation. *Cell* **115**, 333-342 (2003).

40. Hauler, F., Mallery, D.L., McEwan, W.A., Bidgood, S.R. & James, L.C. AAA ATPase p97/VCP is essential for TRIM21-mediated virus neutralization. *Proc Natl Acad Sci U S A* **109**, 19733-19738 (2012).

41. Hanzelmann, P. & Schindelin, H. The Interplay of Cofactor Interactions and Post-translational Modifications in the Regulation of the AAA+ ATPase p97. *Front Mol Biosci* **4**, 21 (2017).

42. Honke, N. *et al.* Enforced viral replication activates adaptive immunity and is essential for the control of a cytopathic virus. *Nat Immunol* **13**, 51-57 (2011).

43. Junt, T. *et al.* Subcapsular sinus macrophages in lymph nodes clear lymph-borne viruses and present them to antiviral B cells. *Nature* **450**, 110-114 (2007).

44. Seifert, U. *et al.* Immunoproteasomes preserve protein homeostasis upon interferon-induced oxidative stress. *Cell* **142**, 613-624 (2010).

45. Papadopoulos, C. *et al.* VCP /p97 cooperates with YOD 1, UBXD 1 and PLAA to drive clearance of ruptured lysosomes by autophagy. *The EMBO Journal* **36**, 135-150 (2016).

46. Zhu, K. *et al.* The phosphorylation and dephosphorylation switch of VCP/p97 regulates the architecture of centrosome and spindle. *Cell Death Differ* **29**, 2070-2088 (2022).

47. Jumper, J. *et al.* Highly accurate protein structure prediction with AlphaFold. *Nature* **596**, 583-589 (2021).

48. Pokhrel, R., Shakya, R., Baral, P. & Chapagain, P. Molecular Modeling and Simulation of the Peptidoglycan Layer of Gram-Positive Bacteria Staphylococcus aureus. *J Chem Inf Model* **62**, 4955-4962 (2022).

49. Huang, J. *et al.* CHARMM36m: an improved force field for folded and intrinsically disordered proteins. *Nat Methods* **14**, 71-73 (2017).